Theory of probing attosecond electron wave packets via two-path interference of angle-resolved photoelectrons

N. N. Choi,[1,2,*] T. F. Jiang,[2,3] T. Morishita,[4,5] M.-H. Lee,[1] and C. D. Lin[2]

[1]*School of Natural Science, Kumoh National Institute of Technology, Gumi, Gyeongbuk 730-701, Korea*

[2]*J. R. Macdonald Laboratory, Physics Department, Kansas State University, Manhattan, Kansas 66506-2604, USA*

[3]*Institute of Physics, National Chiao Tung University, Hsinchu 30010, Taiwan*

[4]*Department of Applied Physics and Chemistry, University of Electro-Communications, 1-5-1 Chofu-ga-oka, Chofu-shi, Tokyo, 182-8585, Japan*

[5]*PRESTO, Japan Science and Technology Agency, Kawaguchi, Saitama 332-0012, Japan*

(Received 6 May 2010; published 15 July 2010)

We study theoretically the electron wave packet generated by an attosecond pulse train (APT) which is probed with a time-delayed infrared (IR) laser pulse. The APT creates an excited state and a continuum electron wave packet. By ionizing the excited state with an IR, a delayed new continuum electron wave packet is created. The interference of the wave packets from the two paths, as reflected in angle-resolved photoelectron spectra, is analyzed analytically. Using the analytical expressions, we examine the possibility of retrieving information on the electron wave packet generated by the APT.

DOI: 10.1103/PhysRevA.82.013409 PACS number(s): 32.80.Rm, 32.80.Qk, 42.65.Ky

I. INTRODUCTION

In recent years attosecond pulse trains (APT) in the extreme ultraviolet (XUV) region have been produced in the process of high-order harmonic generation (HHG) by exposing rare gas atoms to intense femtosecond infrared (IR) laser pulses. These APTs can span a broad spectrum of harmonics, each with a relatively narrow bandwidth, and in the time domain, a series of attosecond bursts of radiation. Thus APT is suitable for initiating a dynamical atomic or molecular system which evolves nontrivially in time, while retaining spectral sensitivity [1,2]. To probe a wave packet created by an APT in the laboratory, the most accessible tools are IR pulses that were employed to generate the APT, or the second or third harmonics of the IR. Such experiments have the advantage that the time delay between the APT and the IR can be controlled with high precision at the level of attoseconds. Attoseconds is also the timescale needed in order to probe the electron wave packet dynamics generated by the APT. The technology for producing APT or single attosecond pulses (SAP) is still in its infancy. Thus, today only a handful of laboratories are capable of performing APT + IR or SAP + IR experiments. Ideally, the goal of a pump-probe experiment is to unravel the dynamic system after the pump. Since the dynamic system evolves in time, the probe pulse has to be applied at different time delays. While it may be of interest to observe how the results of the probe change with time delay, a more interesting and challenging question is to use the results of the probe pulses to retrieve information on the dynamic system after the pump pulse. In this paper we set out to address this question.

In quantum mechanics, each measurement is a projection of the dynamic system. Clearly, not all the probe pulses are equally effective in probing the wave packet generated by the pump. To retrieve the wave packet, equally important is that there should be a well-established simple theory for describing the pump-probe measurements. In this paper we study the wave packet generated by an APT using the helium atom as the target. An IR will be used to probe the resulting wave packet. Such experiments have been carried out already in [3–7], in which the emphasis was on electron wave packet interference where the APT and IR overlap in the time domain. In the APT and IR overlapping region, it is difficult in principle to separate the role of APT and IR in the creation of the electron wave packet. In other words, the IR is not used to probe the wave packet generated by the APT directly. Similar experiment has been reported using single attosecond pulses to excite and ionize H_2 molecules and probed with the IR [8]. Due to the complexity of the excitation pathways in H_2, theoretical analysis of the experimental results is quite a challenge.

For the ultimate goal of retrieving the details of the wave packet created by the APT, in this paper we will consider the helium atom excited and ionized by an APT. After the APT pulse is over, the evolution of the helium atom will be probed by an IR at different delay times and angle-resolved photoelectrons can be determined. Theoretically such a simple system can be solved "exactly" from the numerical solution of the time-dependent Schrödinger equation (TDSE) [9] in the single active electron model [10]. On the other hand, we will show that the electron spectra for such a pump-probe system can be calculated semianalytically. The results from such calculations are compared to the "experimental data" from the numerical TDSE calculation to test the validity of the semianalytical theory we developed in this paper. The theory is described in Sec. II. In Sec. III, angle-resolved electron spectra generated from solving TDSE and from the model will be compared. And, based on the simple model, dependence of angular distribution on the time delay will be investigated. Using the analytical theory we show how partial retrieval of the electron wave packets generated from the APT can be obtained. We finish the paper with a short summary in Sec. IV.

*nnchoi@kumoh.ac.kr

 ©2010 The American Physical Society

II. TWO-PATH INTERFERENCE MODEL FOR PUMP-PROBE EXPERIMENTS

A schematic "experiment" is indicated in Fig. 1(a). We assume the APT is synthesized from the harmonics of a Ti:sapphire laser with a wavelength around 800 nm. A filter is used to select only the harmonics of order 11th–19th. The frequencies of the harmonics can be slightly tuned by changing the gas pressure, laser intensity, and laser frequency [11]. We assume that, by exposing a helium atom to such an APT, the $1s3p\ ^1P$ state (excitation energy is 23.09 eV) is populated prominently among the excited states since we can make the 15th harmonics to be resonant with this level by using the tuning technique mentioned above. In the meanwhile, the 17th and 19th harmonics will ionize the He atom directly to the continuum, generating photoelectrons with mean energy at around 1.55 and 4.55 eV, respectively. Clearly the efficiency of populating the $3p$ state (abbreviated for $1s3p$) and the width of the photoelectron spectra depend on the pulse duration of the APT. After the pulse is over, the 800-nm probe laser is applied to the target atom again. The $3p$ state can be ionized by this probe pulse. The electron wave packet produced through two-photon (four-photon) absorption from the $3p$ state interferes with the wave packet generated directly from the 17th (19th) harmonics. The electron spectra are expected to show interference due to the two paths taken for the electron to reach the same kinetic energy after the probe.

Figure 1 depicts such an experiment. For clarity, we define $t = 0$ to be at the center of the APT pulse. The time difference between the APT and the IR is defined as the time delay, τ. The various parameters of the APT and the IR are clearly defined in Fig. 1(b). For such a dynamic system, the Hamiltonian, written

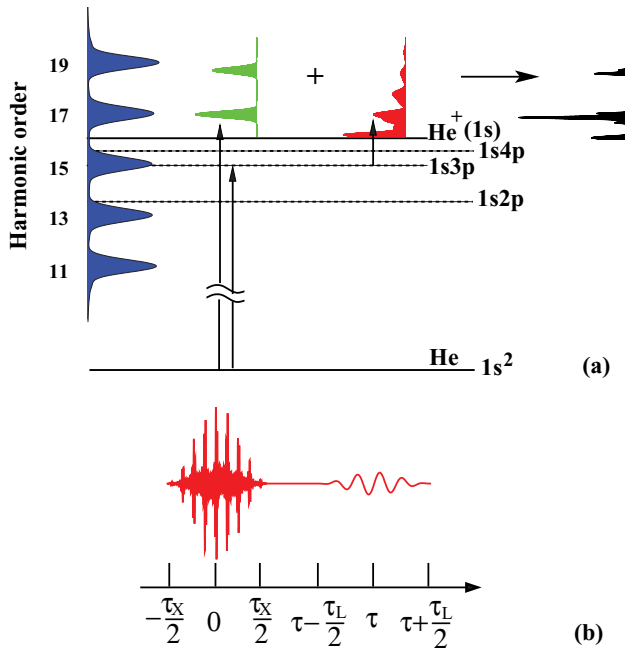

FIG. 1. (Color online) Schematic of two-path interference in API + IR experiment. (a) The energy levels and continuum states involved. (b) Parameters of pump and probe pulses used.

in the dipole approximation, is

$$H(t) = H_0 + zE_X(t) + zE_L(t-\tau), \tag{1}$$

where H_0 is the field-free atomic Hamiltonian, $E_X(t)$ and $E_L(t-\tau)$ are, respectively, the APT pump field and the delayed IR laser field. Here we assumed that all the external fields were polarized along the z axis. Atomic units are used throughout this article unless explicitly stated. For each time delay τ, the time-dependent Schrödinger equation can be solved numerically and the electron momentum spectra are obtained. For each new time delay, the TDSE is solved once again. This way angle-resolved electron spectra versus the time delay can be obtained. Such "exact" numerical solutions, however, do not address the interference of the two pathways described earlier directly. Instead, here we develop a model where the time delay dependence is given analytically.

Considering only the situation in which the pump and probe pulses do not overlap, we can write the total evolution operator for the whole pump-probe cycle as

$$U_{\text{total}} = U\left[\tau + \frac{\tau_L}{2}, \tau - \frac{\tau_L}{2}; E_L(t-\tau)\right] U\left(\tau - \frac{\tau_L}{2}, \frac{\tau_X}{2}; 0\right) \times U\left[\frac{\tau_X}{2}, -\frac{\tau_X}{2}; E_X(t)\right],$$

where $U[t_2,t_1;F(t)]$ represents the evolution operator of the system under an external field $F(t)$ during a time interval from t_1 to t_2. $F(t) = 0$ means the evolution in a free field. For convenience, we define the propagators:

$$U_X \equiv U\left[\frac{\tau_X}{2}, -\frac{\tau_X}{2}; E_X(t)\right], \tag{2}$$

$$U_L \equiv U\left[\tau + \frac{\tau_L}{2}, \tau - \frac{\tau_L}{2}; E_L(t-\tau)\right], \tag{3}$$

such that

$$U_{\text{total}} = U_L e^{-i(\tau - \tau_L/2 - \tau_X/2)H_0} U_X. \tag{4}$$

Representing the atomic evolution operator $\exp[-i(\tau - \tau_L/2 - \tau_X/2)H_0]$ in terms of the bound and continuum eigenstates $|n\rangle$ and eigenenergies ϵ_n of H_0,

$$e^{-i(\tau-\tau_L/2-\tau_X/2)H_0} = \sum_n |n\rangle e^{-i(\tau-\tau_L/2-\tau_X/2)\epsilon_n}\langle n|, \tag{5}$$

we can write the probability amplitude as a function of the time delay τ for transition from initial bound state $|i\rangle$ to an ionized state with photoelectron momentum $\mathbf{p}$ as

$$M_{\mathbf{p}i}(\tau) = \sum_n e^{-i(\tau-\tau_L/2-\tau_X/2)\epsilon_n} M^{(L)}_{\mathbf{p}n} M^{(X)}_{ni}, \tag{6}$$

where $M^{(X)}_{ni}$ and $M^{(L)}_{\mathbf{p}n}$ are probability amplitudes for transitions induced by XUV and IR pulses, respectively,

$$\begin{aligned} M^{(X)}_{ni} &= \langle n|U_X|i\rangle \\ M^{(L)}_{\mathbf{p}n} &= \langle \mathbf{p}|U_L|n\rangle. \end{aligned} \tag{7}$$

Here (and throughout this article) $|\mathbf{p}\rangle$ does not denote a plane wave but a scattering wave which is an eigenstate of H_0 with incoming boundary conditions [12]. From the expression (6) we can interpret the ionization process under the pump probe as a coherent sum of paths represented by the intermediate states n.

Using the identity,

$$U_L \equiv U\left(\tau+\frac{\tau_L}{2},\tau-\frac{\tau_L}{2};E_L(t-\tau)\right)=U\left(\frac{\tau_L}{2},-\frac{\tau_L}{2};E_L(t)\right),$$

we note that the ionization amplitudes $M^{(L)}_{\mathbf{p}n}$ from the intermediate state $|n\rangle$ by the probe pulse is independent of the time delay τ. This means $M_{\mathbf{p}i}$ depends on the time delay τ only through the factor $e^{-i\tau\epsilon_n}$ in Eq. (6). Once τ-independent factors $M^{(L)}_{\mathbf{p}n}$ and $M^{(X)}_{ni}$ are obtained, then we can generate the pump-probe interferogram $|M_{\mathbf{p}i}(\tau)|^2$ as a function of τ for a given momentum $\mathbf{p}$ by using Eq. (6).

For a helium atom in the ground state exposed to the APT introduced previously, the transition amplitude $M^{(X)}_{ni}$ for bound states other than $n=3p$ is negligible. Thus, $M_{\mathbf{p}i}(\tau)$ can be approximately written as

$$M_{\mathbf{p}i}(\tau)=e^{-i(\tau-\tau_L/2-\tau_X/2)\epsilon_{3p}}M^{(L)}_{\mathbf{p},3p}M^{(X)}_{3p,i}+\int d^3\mathbf{p}'e^{-i(\tau-\tau_L/2-\tau_X/2)\epsilon_{\mathbf{p}'}}M^{(L)}_{\mathbf{p}\mathbf{p}'}M^{(X)}_{\mathbf{p}'i}, \quad (8)$$

where the second term on the right-hand side represents the contribution from the intermediate scattering states $|\mathbf{p}'\rangle$. Since energy and momentum of a free electron are not changed by a laser field, the IR introduces a Volkov phase [13] only. Thus, we employ an approximation,

$$M^{(L)}_{\mathbf{p}\mathbf{p}'}\approx\delta(\mathbf{p}-\mathbf{p}')\exp\left\{-\frac{i}{2}\int_{-\tau_L/2}^{\tau_L/2}[\mathbf{p}+\mathbf{A}(t)]^2\,dt\right\}, \quad (9)$$

where $\mathbf{A}$ is the vector potential describing the IR probe laser pulse.

Using this approximation, $M_{\mathbf{p}i}$ can be written as a coherent sum of contributions from the two paths,

$$M_{\mathbf{p}i}(\tau)=e^{-i(\tau-\tau_L/2-\tau_X/2)\epsilon_{3p}}M^{(L)}_{\mathbf{p},3p}M^{(X)}_{3p,i}+e^{-i(\tau-\tau_L/2-\tau_X/2)\epsilon_{\mathbf{p}}}e^{-i(\tau_L\epsilon_{\mathbf{p}}+\alpha\cdot\mathbf{p}+\beta)}M^{(X)}_{\mathbf{p}i}, \quad (10)$$

where

$$\alpha=\int_{-\tau_L/2}^{\tau_L/2}\mathbf{A}(t)\,dt \quad \text{and} \quad \beta=\frac{1}{2}\int_{-\tau_L/2}^{\tau_L/2}A^2(t)\,dt. \quad (11)$$

Here the transition amplitudes $M^{(L)}_{\mathbf{p},3p}$, $M^{(X)}_{3p,i}$, and $M^{(X)}_{\mathbf{p}i}$ can be, respectively, obtained, for example, by solving the corresponding time-dependent Schrödinger equations. Introducing their magnitudes and phases such that

$$M^{(X)}_{\mathbf{p}i}=a_{\mathbf{p}}e^{i\varphi_{\mathbf{p}}},\quad M^{(X)}_{3p,i}=a_{3p}e^{i\varphi_{3p}},\quad \text{and}\quad M^{(L)}_{\mathbf{p},3p}=b_{\mathbf{p},3p}e^{i\phi_{\mathbf{p},3p}}, \quad (12)$$

the ionization probability density is expressed as

$$|M_{\mathbf{p}i}(\tau)|^2=a^2_{\mathbf{p}}+b^2_{\mathbf{p},3p}a^2_{3p}+2a_{\mathbf{p}}b_{\mathbf{p},3p}a_{3p}\times\cos[\Phi_{\mathbf{p},3p}-(\epsilon_{\mathbf{p}}-\epsilon_{3p})\tau], \quad (13)$$

with

$$\Phi_{\mathbf{p},3p}=\varphi_{\mathbf{p}}-(\epsilon_{\mathbf{p}}\tau_L+\mathbf{p}\cdot\alpha+\beta)-(\varphi_{3p}+\phi_{\mathbf{p},3p})+(\epsilon_{\mathbf{p}}-\epsilon_{3p})(\tau_X+\tau_L)/2. \quad (14)$$

Note that in Eq. (13), the first term gives the probability for producing an electron with momentum $\mathbf{p}$ by the APT. The second term is the probability for the APT to excite helium to $3p$ and for the IR to ionize the helium from the $3p$ to the continuum state with the same final momentum $\mathbf{p}$. The last term is due to the interference of the two paths, where the time delay dependence is explicitly expressed. Note that the phase $\Phi_{\mathbf{p},3p}$ includes the phase of the excitation and ionization amplitudes by the APT, as well as those from $3p$ to the continuum by the IR. It does not depend on the time delay.

III. ANGLE-RESOLVED PHOTOELECTRON SPECTRA

A. The two-path interference model and the TDSE

To illustrate the two-path interference model, we consider a situation where an APT consists of odd harmonics from 11th to 19th as mentioned in the previous section. The amplitude of each harmonic is assumed to be equal. A sine square pulse is used, with full width of half-maximumn (FWHM) of 4.5 fs, and peak intensity of $2\times10^{13}\mathrm{W/cm^2}$. Using helium as the target, we obtained energy spectra of photoelectrons in the direction along the polarization of the pump laser. Photoelectrons generated directly by the 17th and 19th harmonics of the APT are shown as a dash-dotted line in Fig. 2(a). The APT also generate the $3p$ state of helium by the 15th harmonic. Using a delayed IR to ionize helium from $3p$, the photoelectron spectrum is shown as a dotted line in Fig. 2(a). The IR used in this example has wavelength at 819 nm, 5-fs FWHM, peak intensity of $10^{13}\mathrm{W/cm^2}$, and carrier-envelop phase of $\pi/2$. Note the presence of above-threshold ionization (ATI) peaks, where the first ATI peak is partially visible only. Due to the short duration, the ATI peaks are not very sharp. The two spectra overlap mostly in the region of the second ATI peak. In obtaining these two electron spectra, TDSE calculations were performed separately for the APT, and the IR. Thus, $M^{(X)}_{3p,i}$, $M^{(X)}_{\mathbf{p}i}$, and $M^{(L)}_{\mathbf{p},3p}$ are obtained. With these amplitudes, the two-path interference model, Eq. (13) allows us to obtain the electron spectra if the IR is applied following by a time

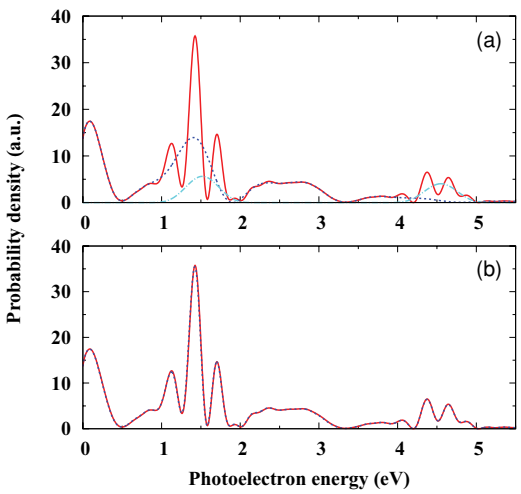

FIG. 2. (Color online) (a) Photoelectron energy spectrum $|M_{\mathbf{p}i}(\tau)|^2$ (denoted by a red solid line) obtained by using the two-path interference model (13) for a specific momentum direction $\theta_{\mathbf{p}}\approx\pi$ and time delay $\tau=5T_0$, where T_0 is the period of single oscillation of the IR laser. Dotted and dash-dotted lines are, respectively, $|M^{(L)}_{\mathbf{p},3p}M^{(X)}_{3p,i}|^2$ and $|M^{(X)}_{\mathbf{p}i}|^2$. (b) Comparison with the "exact" TDSE calculational result (a dotted line).

delay τ after the APT. The photoelectron spectra, shown in Fig. 2(a) as a (red) full line, for $\tau = 5T_0$, demonstrated the consequence of two-path interference. Here, T_0 is the period of single oscillation of the IR laser. To show that the analytical model of Eq. (13) is correct, we also obtain the electron spectra from solving the TDSE directly for the whole APT + IR pulse, so-called the "exact" TDSE, with the same time delay $\tau = 5T_0$. The resulting photoelectron spectra, shown in Fig. 2(b) as a dotted line, show good agreement with the one from the two-path interference model. It further confirms that interference occurs only in the energy region where photoelectrons can be reached by the two paths.

B. Interferences in angular distributions

Equation (13) allows us to predict how the angular distributions for a given electron energy depends on the time delay. Consider the 4th ATI peak, at photoelectron energy of $\epsilon = 0.166$ a.u.$= 4.52$ eV, $(\epsilon_{\mathbf{p}} - \epsilon_{3p}) \approx 4\omega_0$. From Eq. (13), the interference term repeats at every $\tau \approx T_0/4$. Here, $\omega_0 = 2\pi/T_0$ is the photon energy of the IR laser. This result is illustrated in Fig. 3, where the angular distributions are plotted for four different time delays $\tau = 4.75T_0$, $4.875T_0$, $5.0T_0$, and $5.125T_0$. On each curve, there are two data sets where time delays differ by $T_0/4$. For the angular distributions for electron energy near the second ATI peak, it would repeat at every $\tau \approx T_0/2$ as can be easily seen from Eq. (13).

C. Controlling asymmetry of photoelectron emission by pump-probe time delay

In the pump-probe experiments, the two-path interference can produce much larger asymmetry in the angular distribution of the photoelectron even if the separate contributions of the two paths have negligible asymmetries. To effectively demonstrate this, we use the second harmonic of the IR employed to generate the APT as a probe pulse. The FWHM

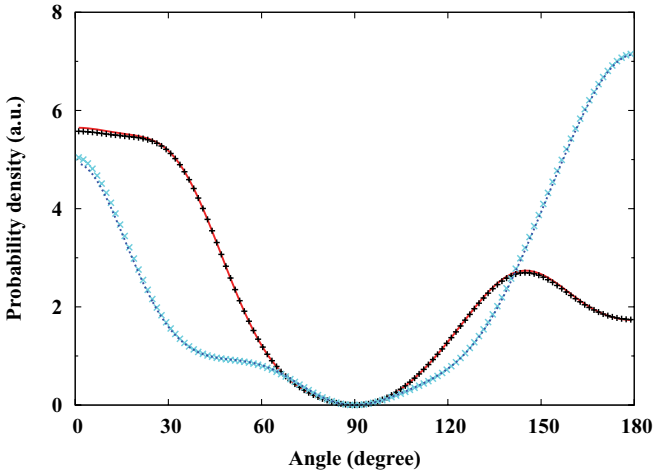

FIG. 3. (Color online) Angular distributions of photoelectron with a fixed energy $\epsilon_{\mathbf{p}} = 0.166$ a.u. for four different time delays $\tau = 4.75T_0$ (red solid line), $4.875T_0$ (dotted), $5.0T_0$ (+), and $5.125T_0$(×). The distributions are identical to each other if the two time delays differ by $T_0/4$. The spectra are for electrons where $(\epsilon_{\mathbf{p}} - \epsilon_{3p}) \approx 4\omega_0$; see text.

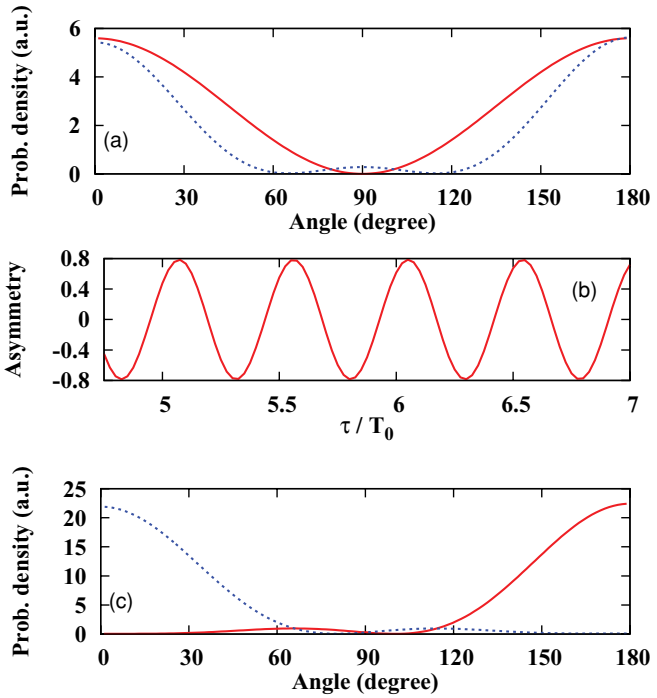

FIG. 4. (Color online) (a) Angular distributions of photoelectron, for a fixed energy $\epsilon_{\mathbf{p}} = 0.0566$ a.u., directly generated by absorption of the 17th harmonics (red solid line) and produced through single-photon absorption of the second harmonics from $3p$ state (blue dotted line). (b) Asymmetry $A(\epsilon)$, as a function of the time delay for $\epsilon_{\mathbf{p}} = 0.0566$ a.u., in the angular distribution of photoelectron produced in the pump-probe experiment using the second harmonics as a probe. (c) Angular distributions of photoelectron corresponding to the time delays $\tau = 4.825T_0$ (red solid line) and $5.075T_0$ (blue dotted line) in (b).

and peak intensity is, respectively, chosen to be 5 fs and 3×10^{12} W/cm^2. Figure 4(a) shows the angular distributions of the photoelectrons produced separately by the two paths (i.e., $a_{\mathbf{p}}^2$ and $b_{\mathbf{p},3p}^2 a_{3p}^2$ for $\epsilon = 0.0566$ a.u. $= 1.54$ eV); they are almost symmetric, and their magnitude and shape are similar to each other. In fact, at the intensities used here, photoionization from the ground state by APT is a one-photon process, thus the electrons's angular momentum is $l = 1$. The ionization pathway from $3p$ is also a single photon absorption of the second harmonic, and the electron's angular momentum will be either $l = 0$ or 2. By changing the time delay between the two paths, the odd angular function from the direct path and the even angular function from the indirect path can be added constructively on one side of the electron ejection and destructively on the other side, thus creating strong asymmetry in the angular emission of the photoelectrons, as shown in Fig. 4(c).

The sensitivity of angular distributions on the time delay can be conveniently described by the range of variation of the asymmetry parameter $A(\epsilon)$ which is defined as the difference in signal between the top and bottom half of the momentum distribution at a particular photoelectron energy ϵ,

$$A(\epsilon) = \frac{n_{\text{up}} - n_{\text{down}}}{n_{\text{up}} + n_{\text{down}}}. \tag{15}$$

Using such a definition we can show the asymmetry of up-down electrons versus time delay. Figure 4(b) shows the

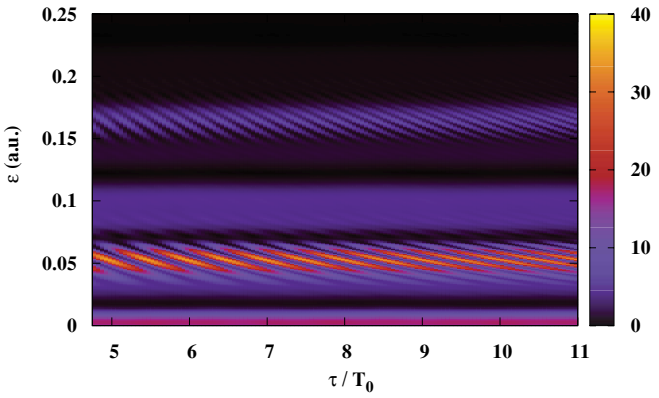

FIG. 5. (Color online) Interferogram $I(\epsilon_{\mathbf{p}},\tau)$, that is, photoelectron two-dimensional spectrum in τ-$\epsilon_{\mathbf{p}}$ space for a specific momentum direction $\theta_{\mathbf{p}} \approx \pi$. The data were obtained by using the "exact" TDSE calculation for each time delay.

large asymmetry of the directional electron emission. Thus, using two-path interference, it offers an efficient means of generating strong directional continuum electrons, simply just by tuning the time delay between the pump-probe pulses. To our knowledge, this is a much more efficient way for creating electrons in preferential directions by photons than using few-cycle pulses [14–16].

D. Two-path interfering electron spectra versus time delay at a fixed emission angle

From Fig. 3 we note that the angular distribution tends to peak along the polarization axis. Thus it is pertinent to examine the electron spectra at a fixed angle near 0 or π and display the energy-τ spectra (i.e., $|M_{\mathbf{p}i}(\tau)|^2$), at the fixed angle, which will be denoted by $I(\epsilon,\tau)$. Figure 5 shows the spectra at an angle near π. Clear interference fringes can be seen for each narrow energy range around the second and fourth ATI peaks. Based on the two-path interference model, these fringes can be understood easily. Clearly from Eq. (13), for a fixed emission angle, the peak of the spectra occurs when

$$\Phi_{\mathbf{p},3p} - (\epsilon_{\mathbf{p}} - \epsilon_{3p})\tau = 2n\pi, \tag{16}$$

where n is a positive or negative integer. Within a narrow energy region, say near the second or the fourth ATI peak, from Eq. (14), we expect $\Phi_{\mathbf{p},3p}$ be approximated by a constant (unless there are resonances within the energy region). Under this approximation, the fringe will be a hyperbola in the $I(\epsilon,\tau)$ plot. Such $I(\epsilon,\tau)$ is similar to the interferogram in optics. The density of the fringe, from Eq. (13), depends on the value of $(\epsilon - \epsilon_{3p})$. For the band near the fourth ATI peak, its value is about twice that of the band near the second ATI peak. Thus the fringe repeats at about twice the rate for the former compared to the latter band for the same range of τ. For each band, the density of the fringe increases for larger τ. Each fringe is tilted toward smaller τ with increasing electron energy. All of these features can be easily understood from Eq. (16). We comment that if $\Phi_{\mathbf{p},3p}$ is a strict constant, then the hyperbola in the fourth ATI peak region should connect smoothly with the hyperbola in the second ATI peak region. This is not the case since $\Phi_{\mathbf{p},3p}$ is expected to be different over a larger energy region. We comment that similar analysis of $I(\epsilon,\tau)$ has been done earlier [17,18] without the benefit of the analytical expression Eq. (13).

IV. PARTIAL RETRIEVAL OF ELECTRON WAVE PACKET

After identifying that the function $I(\epsilon,\tau)$ is similar to the interferogram in optics, we can follow optics to use its Fourier integral transform, defined by

$$F(\epsilon,\epsilon') = \frac{1}{\tau_f - \tau_i}\int_{\tau_i}^{\tau_f} d\tau\, I(\epsilon,\tau)e^{i\epsilon'\tau}, \tag{17}$$

to retrieve information about the composition of the wave packet. Writing $I(\epsilon,\tau)$ [See Eq. (13)] in the form of

$$I(\epsilon,\tau) = I_{\mathrm{bg}}(\epsilon) + 2I_{\mathrm{os}}(\epsilon)\cos[\Phi_{\mathbf{p},3p} - (\epsilon - \epsilon_{3p})\tau], \tag{18}$$

with

$$I_{\mathrm{bg}}(\epsilon) = a_{\mathbf{p}}^2 + b_{\mathbf{p},3p}^2 a_{3p}^2, \tag{19}$$

$$I_{\mathrm{os}}(\epsilon) = a_{\mathbf{p}} b_{\mathbf{p},3p} a_{3p}, \tag{20}$$

we can easily obtain

$$\begin{aligned} F(\epsilon,\epsilon') = {} & I_{\mathrm{bg}}(\epsilon)e^{i\epsilon'(\tau_f+\tau_i)/2}\mathrm{sinc}[\epsilon'(\tau_f - \tau_i)/2] \\ & + I_{\mathrm{os}}(\epsilon)\{e^{i\Phi_{\mathbf{p},3p}}e^{-i(\epsilon-\epsilon_{3p}-\epsilon')(\tau_f+\tau_i)/2} \\ & \times \mathrm{sinc}\,[(\epsilon - \epsilon_{3p} - \epsilon')(\tau_f - \tau_i)/2] \\ & + e^{-i\Phi_{\mathbf{p},3p}}e^{i(\epsilon-\epsilon_{3p}+\epsilon')(\tau_f+\tau_i)/2} \\ & \times \mathrm{sinc}\,[(\epsilon - \epsilon_{3p} + \epsilon')(\tau_f - \tau_i)/2]\}. \end{aligned} \tag{21}$$

Here $(\tau_f - \tau_i)$ is the range of pump-probe time delay measured in the experiment, and $\mathrm{sinc}(x) = \sin(x)/x$. Recall that $\mathrm{sinc}(x)$ is a damped oscillating function peaked at $x = 0$ and the width of the peak of $\mathrm{sinc}[\epsilon(\tau_f - \tau_i)/2]$ in ϵ space decreases as $(\tau_f - \tau_i)$ increases such that

$$\mathrm{sinc}\,[\epsilon(\tau_f - \tau_i)/2] \to 0 \quad \text{for} \quad \epsilon \neq 0 \ \text{ as } (\tau_f - \tau_i) \to \infty. \tag{22}$$

Thus, as the range of time delay increases, the magnitude of $F(\epsilon,\epsilon')$ can be large only on the three straight lines: $\epsilon' = 0$ from the first term, $\epsilon - \epsilon_{3p} - \epsilon' = 0$ from the second term, and $\epsilon - \epsilon_{3p} + \epsilon' = 0$ from the last term of the right-hand side in Eq. (21). A plot of $|F(\epsilon,\epsilon')|$ in the (ϵ',ϵ) plane is presented in Fig. 6, where we can clearly see the peaks along the vertical line $\epsilon' = 0$ and those on a straight line with an inclination angle $\pi/4$. The latter line is considered to be described by $\epsilon = \epsilon' + \epsilon_{3p}$ in accordance with the peak positions of the second term in Eq. (21). The value of ϵ_{3p} can be retrieved from this figure by fitting the line to the equation $\epsilon - \epsilon_{3p} - \epsilon' = 0$ such that $\epsilon_{3p} = -0.0568$ a.u., which is the same as the exact value obtained by solving the time-independent Schrödinger equation for bound states. Note that the line $\epsilon - \epsilon_{3p} + \epsilon' = 0$ lies out of the energy region considered in this figure.

In addition to the bound state energy ϵ_{3p}, we can retrieve the incoherent background amplitude $I_{\mathrm{bg}}(\epsilon)$ and the amplitude of the oscillation $I_{\mathrm{os}}(\epsilon)$ from $|F(\epsilon,\epsilon')|$. To demonstrate this, we show a plot of $|F(\epsilon,\epsilon')|$ as a function of ϵ' at a given $\epsilon = 0.166$ a.u. in Fig. 7(a). The peak value read from this figure at $\epsilon' = 0$ is 4.459, compared to the calculated value $I_{\mathrm{bg}}(\epsilon) = 4.459$ using Eq. (19), while the peak value read at $\epsilon' = \epsilon - \epsilon_{3p} =$

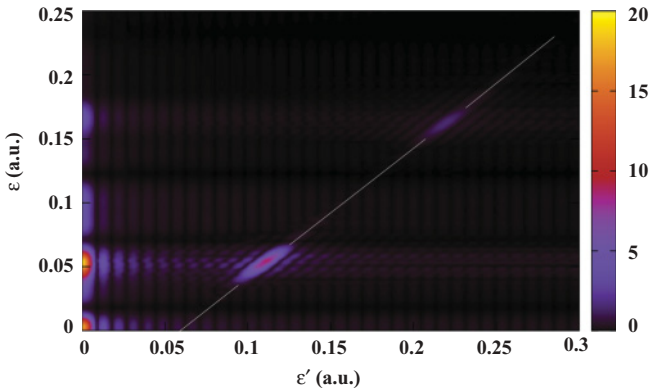

FIG. 6. (Color online) Magnitude of the Fourier integral transform $F(\epsilon,\epsilon')$ of the interferogram $I(\epsilon_{\mathbf{p}},\tau)$ at a fixed direction $\theta \approx \pi$. Peaks can be clearly seen along two lines; one is the vertical line at $\epsilon' = 0$ and the other is a straight line (indicated by white segments) with an inclination angle $\pi/4$.

$0.166 + 0.0569 = 0.2228$ is 1.384 and the theoretical value from Eq. (20) is $I_{\rm os} = 1.391$. The small difference is due to the fact that the range of τ, $(\tau_f - \tau_i)$, in Eq. (17) covered in Fig. 5, is about 700 a.u. only. Thus $\mathrm{sinc}[\epsilon(\tau_f - \tau_i)/2]$ does not approach the asymptotic limit as in Eq. (22) yet. Such finite range τ integration in Eq. (17) also reflects the minor interference structures observed in Fig. 6 between the lines $\epsilon' = 0$ and $\epsilon = \epsilon' + \epsilon_{3p}$. We comment that similar analysis have been used previously for SAP + IR experiments on He [17,18] and on H_2 [8].

From Eq. (21), we note that the phase of $F(\epsilon,\epsilon')$ can be used to obtain the phase $\Phi_{\mathbf{p},3p}$. In Fig. 7(b) we show the phase of $F(\epsilon,\epsilon')$ as a function of ϵ' at a given energy $\epsilon = 0.166$ a.u.. As can be seen from the phase factors in the second term in

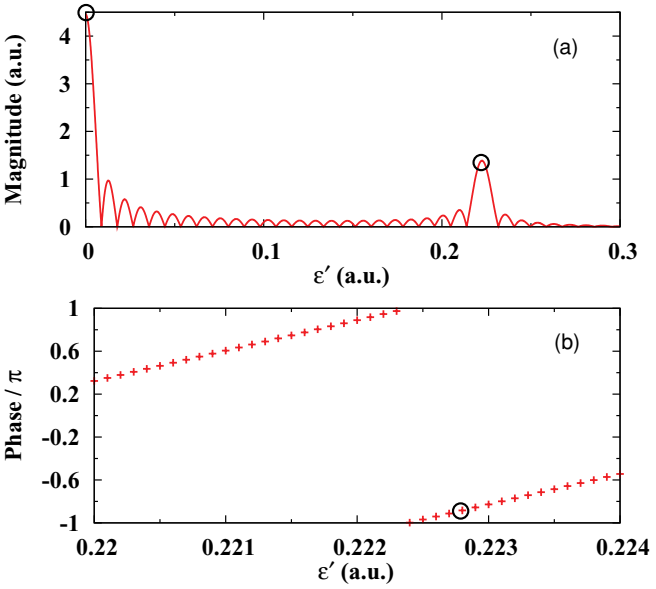

FIG. 7. (Color online) (a) A cut of $|F(\epsilon,\epsilon')|$ at a given $\epsilon = 0.166$ a.u., as a function of ϵ'. The peaks at $\epsilon' = 0$ and 0.2228 are denoted by circles. (b) A cut of phase of $F(\epsilon,\epsilon')$ at the same ϵ as in (a). The data point corresponding to the phase at $\epsilon' = 0.2228$ is denoted by a circle.

Eq. (21), $\Phi_{\mathbf{p},3p}$ at $\epsilon = 0.166$ a.u. can be retrieved by reading the phase of $F(\epsilon = 0.166,\epsilon')$ at $\epsilon' = \epsilon - \epsilon_{3p} = 0.2228$ a.u.. The value read from Fig. 7(b) is -0.88π, in good agreement with the value calculated from using Eq. (14).

Based on the above discussion, from the Fourier integral transform of the interferogram $I(\epsilon,\tau)$ measured at a given angle, one can only obtain partial information such as $a_{\mathbf{p}}$, $b_{\mathbf{p},3p}a_{3p}$, $\Phi_{\mathbf{p},3p}$, and ϵ_{3p}. It is not possible to retrieve the full information of the wave packet generated by the pump beam (i.e., $a_{\mathbf{p}}$, a_{3p}, and $\varphi_{\mathbf{p}} - \varphi_{3p}$). If the interaction of the probe beam with the target is weak such that perturbation theory will work and thus all terms in Eq. (14) involving the probe pulse are known, then knowledge of $\Phi_{\mathbf{p},3p}$ would allow the determination of $\varphi_{\mathbf{p}} - \varphi_{3p}$ [see Eq. (14)]. Under this ideal condition, then, from the time-delayed pump-probe measurements, the electron wave packet generated by the APT can be reconstructed from the measured interferogram $I(\epsilon,\tau)$. If the probe is not a perturbation, any measurement would introduce additional unknowns. While partial information on the electronic wave packet can be obtained using a probe pulse, full characterization of the wave packet generated by a pump beam will be extremely challenging.

Before closing, we mention that angle-resolved photoelectron spectra in APT + IR experiments are still very few. Spectra similar to Fig. 6 have been shown in [17]. Experiments using SAP instead of APT and probed by IR have also been reported recently using H_2 target [8] as well as He target [18]. Clearly the present theory can be extended to SAP + IR experiments. A large bandwidth of a SAP leads to the excitation of a broad coherent superposition of states. It is remarkable that Eqs. (6) and (9) remain intact for these experiments if only the pulses do not overlap. Applying these equations and following the steps similar to Eqs. (10)–(14), one can easily understand the two-path interference signals in the Fourier transform of the angle-resolved photoelectron spectrum; in addition to the peaks along straight lines with an inclination angle $\pi/4$ as in the present APT + IR experiment, the interference between two paths passing through different excited states $|n\rangle$ and $|m\rangle$ gives rise to peaks along a vertical line at $\epsilon' = |\epsilon_n - \epsilon_m|$. The vertical lines in the insets of Fig. 3 in Ref. [8] and those denoted by "QB" in Fig. 2(b) in Ref. [18] show this type of two-path interference. It is noted that there is no peak along a straight line with an inclination of $\pi/4$ in the inset of Fig. 3 in Ref. [8] because the SAP in that experiment creates only a coherent superposition of vibrational states of H_2^+ without molecular dissociation.

V. SUMMARY

In this paper we introduce a simple theory which treats the free evolution of the quantum mechanical system analytically in a typical pump-probe experiment employing nonoverlapping pulses. The validity of the theory was confirmed by comparing to angle-resolved photoelectron energy spectra calculated from solving TDSE. The analytic theory illustrates the interference of the different pathways for the electron emission directly. From the evolution of the angle-resolved electron spectra versus the time delay, we show that partial information of the wave packet generated by the pump beam can be extracted. However, to retrieve the whole wave packet even for the simplified system treated here proves to be rather

difficult. On the other hand, we show that the directional photoelectron emission can be nicely controlled using the two-path interference method, by simply tuning the time delay between the pump and probe pulses. This may lead to a powerful coherent control of the electron wave packet [19].

ACKNOWLEDGMENTS

This work was supported in part by Chemical Sciences, Geosciences and Biosciences Division, Office of Basic Energy Sciences, Office of Science, US Department of Energy. N.N.C. was supported by National Research Foundation of Korea under Contract No. KRF-2008-314-C00076 and Research Foundation of Kumoh National Institute of Technology; T.F.J. was supported by the National Science Council of Taiwan under Contract No. NSC97-2112-M-009-002-MY3. T.M. was supported in part by a Grant-in-Aid for Scientific Research (C) from the Ministry of Education, Culture, Sports, Science and Technology, Japan.

[1] P. M. Paul *et al.*, Science **292**, 1689 (2001).
[2] P. Tzallas *et al.*, Nature **426**, 267 (2003).
[3] P. Johnsson *et al.*, Phys. Rev. Lett. **95**, 013001 (2005).
[4] T. Remetter *et al.*, Nat. Phys. **2**, 323 (2006).
[5] P. Johnsson, J. Mauritsson, T. Remetter, A. L'Huillier, and K. J. Schafer, Phys. Rev. Lett. **99**, 233001 (2007).
[6] P. Ranitovic *et al.*, New J. Phys. **12**, 013008 (2010).
[7] X. M. Tong, P. Ranitovic, C. L. Cocke, and N. Toshima, Phys. Rev. A **81**, 021404(R) (2010).
[8] F. Kelkensberg *et al.*, Phys. Rev. Lett. **103**, 123005 (2009).
[9] T. Morishita, Z. Chen, S. Watanabe, and C. D. Lin, Phys. Rev. A **75**, 023407 (2007).
[10] X. M. Tong and C. D. Lin, J. Phys. B **38**, 2593 (2005).
[11] H. T. Kim, D. G. Lee, K. H. Hong, J. H. Kim, I. W. Choi, and C. H. Nam, Phys. Rev. A **67**, 051801(R) (2003).
[12] C. J. Joachain, *Quantum Collision Theory* (North-Holland, Amsterdam, 1975), Chapter 6.
[13] D. M. Volkov, Z. Phys. **94**, 250 (1935); H. R. Reiss, Phys. Rev. A **22**, 1786 (1980).
[14] G. G. Paulus *et al.*, Nature (London) **414**, 182 (2001).
[15] S. Micheau, Z. Chen, A. T. Le, J. Rauschenberger, M. F. Kling, and C. D. Lin, Phys. Rev. Lett. **102**, 073001 (2009).
[16] Z. Chen, T. Wittmann, B. Horvath, and C. D. Lin, Phys. Rev. A **80**, 061402(R) (2009).
[17] T. Remetter, Ph.D. thesis, Lund University, 2008.
[18] J. Mauritsson *et al.*, e-print arXiv:1001.1085.
[19] T. C. Weinacht, J. Ahn, and P. H. Bucksbaum, Nature (London) **397**, 233 (1999).